Supporting Information for "Ocean Circulation Signatures of North Pacific Decadal Variability"

Robert C. J. Wills[1]**, David S. Battisti**[1]**, Cristian Proistosescu**[2]**,**

LuAnne Thompson[3]**, Dennis L. Hartmann**[1]**, Kyle C. Armour**[1,3]

[1]Department of Atmospheric Sciences, University of Washington, Seattle, WA
[2]Joint Institute for the Study of the Atmosphere and Ocean, University of Washington, Seattle, WA
[3]School of Oceanography, University of Washington, Seattle, WA

Contents of this file

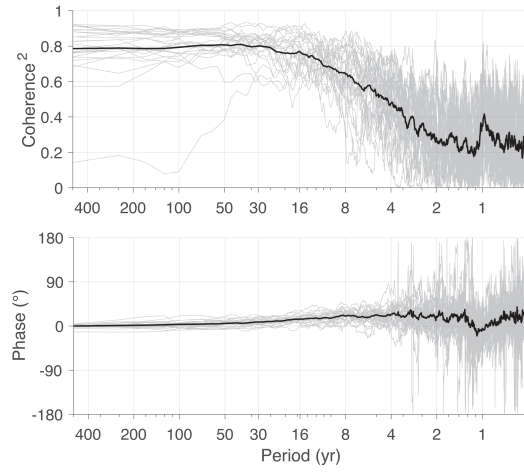Corresponding author: R. C. J. Wills, `rcwills@uw.edu`

Figure S1. Spectral relationships between PC-PDO and LFC-PDO. The top panel shows squared coherence. The bottom panel shows phase (positive where LFC-PDO lags PC-PDO). Black lines show the multi-model mean; grey lines show individual models.
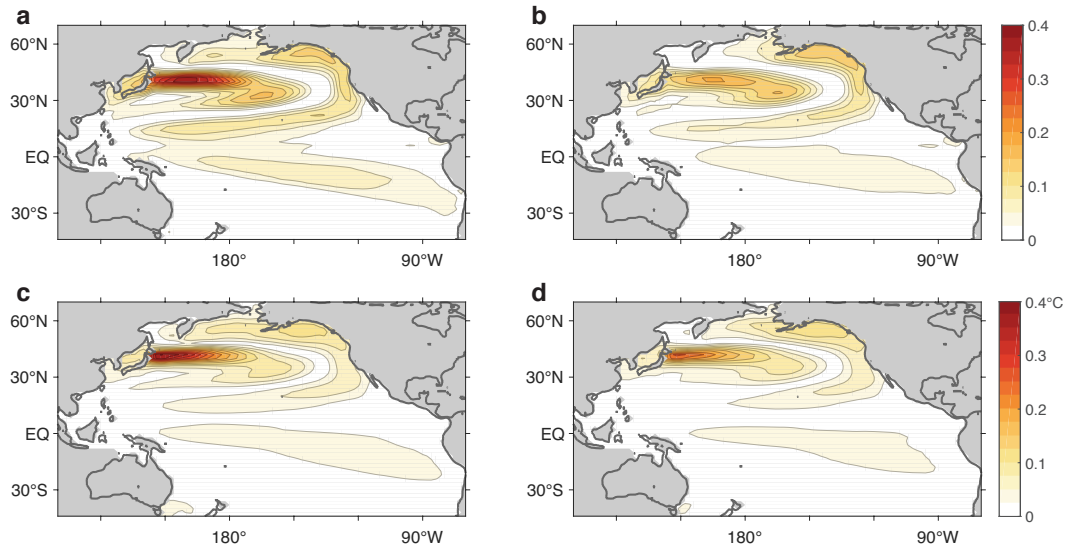

Figure S2. Spatial map of the fraction of decadal running mean variance explained by (a) LFC-PDO and (b) PC-PDO at each grid point. Standard deviation of decadal running mean SST variations (in °C) associated with variability in (c) LFC-PDO and (d) PC-PDO.
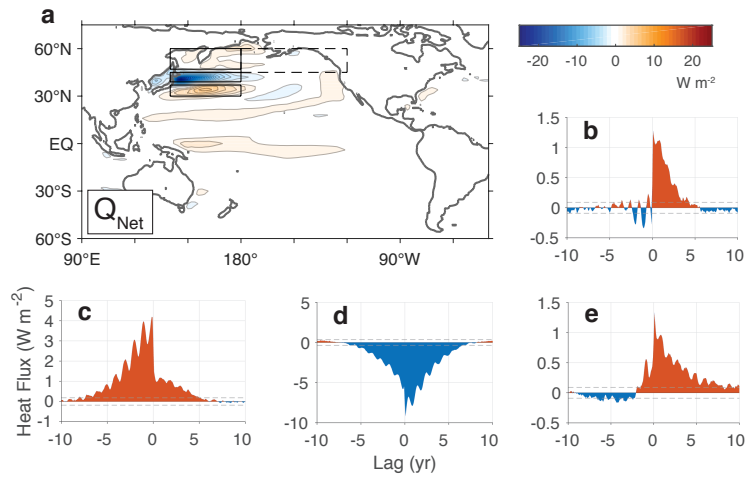
Figure S3. (a) Lag-0 regression of net surface heat flux (including radiative fluxes, positive upwards) onto the LFC-PDO. (b)-(d) Lead-lag regression of net surface heat flux averaged over North Pacific boxes onto the LFC-PDO: (b) the eastern North Pacific and, from south to north, (c) the Kuroshio current, (d) the Oyashio current, and (e) the western North Pacific. Positive (red) indicates heat fluxes from the ocean into the atmosphere. Dashed grey lines show the 95% significance levels, computed using phase randomization [cf. Ebisuzaki, (1997)]. Averaging regions are shown with boxes in panel (a).
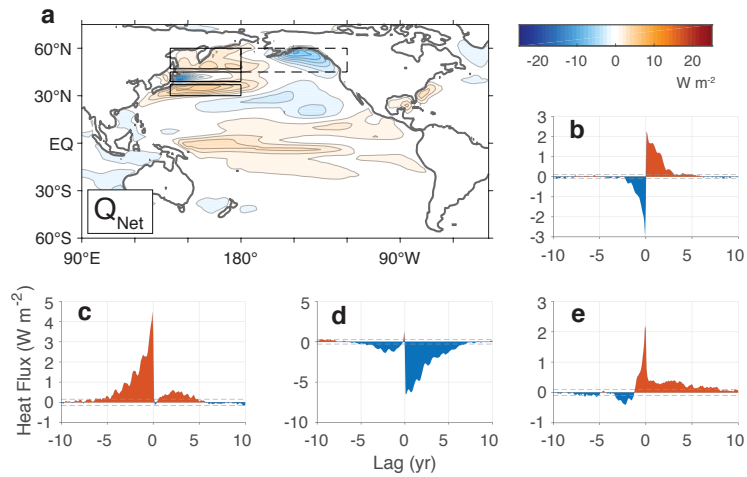

Figure S4. (a) Lag-0 regression of net surface heat flux (including radiative fluxes, positive upwards) onto the PC-PDO. (b)-(d) Lead-lag regression of net surface heat flux averaged over North Pacific boxes onto the PC-PDO: (b) the eastern North Pacific and, from south to north, (c) the Kuroshio current, (d) the Oyashio current, and (e) the western North Pacific. Positive (red) indicates heat fluxes from the ocean into the atmosphere. Dashed grey lines show the 95% significance levels, computed using phase randomization [cf. Ebisuzaki, (1997)]. Averaging regions are shown with boxes in panel (a).
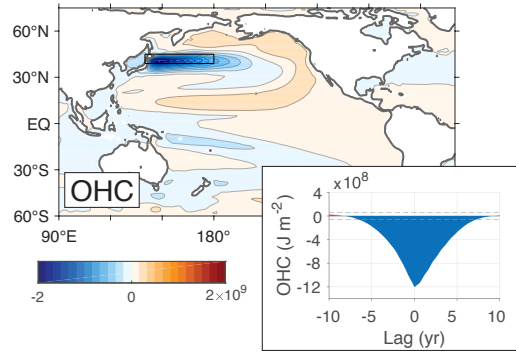
Figure S5. Lag-0 regression of full-column vertically integrated ocean heat content onto the LFC-PDO. The inset shows the lead-lag regression of vertically integrated ocean heat content averaged over the Kuroshio-Oyashio Extension (KOE, 140°E–180°; 39–45°N). Dashed grey lines show the 95% significance levels, computed using phase randomization [cf. Ebisuzaki, (1997)].
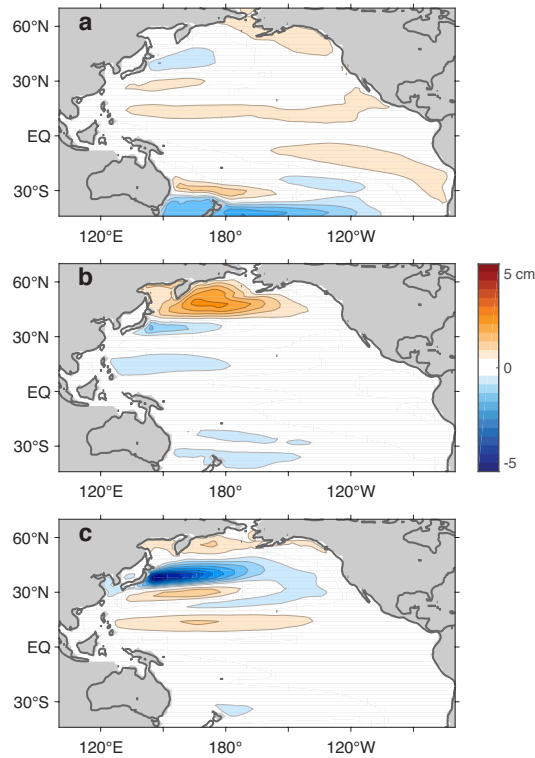

Figure S6. Sea-surface height (SSH) anomaly patterns from LFCA of Pacific SSH anomalies across the 21 CMIP5 models that output SSH (using a 10-year lowpass cutoff and retaining 50 EOFs). (a) Low-frequency pattern (LFP) 1 of Pacific SSH anomalies. (b) LFP 2 of Pacific SSH anomalies. (c) LFP 3 of Pacific SSH anomalies, which is similar to the SSH regression onto the LFC-PDO (Fig. 2d).
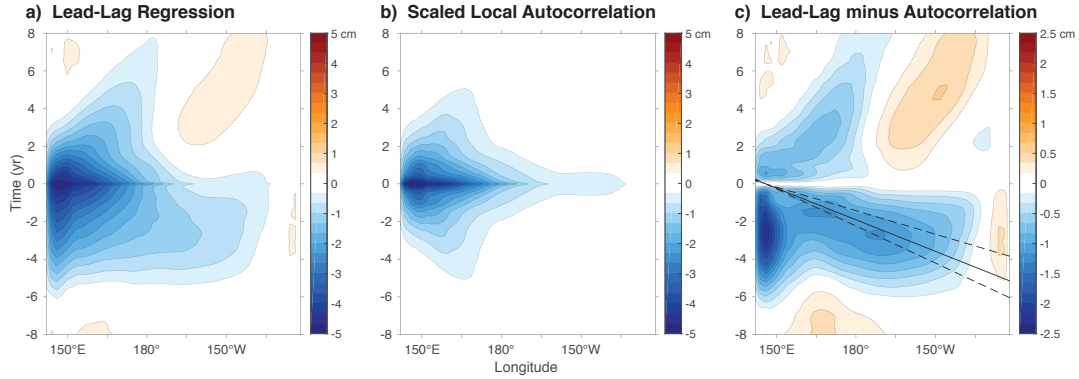
Figure S7. Hovmöller diagrams of SSH anomalies at 38°N. (a) Lead-lag regression of 38°N SSH anomalies onto LFC 3 of Pacific SSH (associated with the SSH pattern in Fig. S6c and highly correlated with the LFC-PDO as shown in Fig. 2d). Positive lag indicates SSH anomalies that lag LFC 3. (b) Lead-lag regression expected from local SSH autocorrelations at 38°N [i.e., point-wise SSH autocorrelation scaled by the lag-0 regression amplitude shown in (a)]. (c) Lead-lag regression minus scaled autocorrelation [i.e., (a) - (b)]. The solid (dashed) black line(s) show anomalies that propagate from the Aleutian low forcing region (∼166°W) to the KOE (∼146°E) in 32 months (24 and 38 months), corresponding to the inter-model median AR(1) timescale and the interquartile range. Persistent anomalies at 146°E are likely indicative of a faster oceanic response (e.g., barotropic) to persistent Aleutian low forcing.
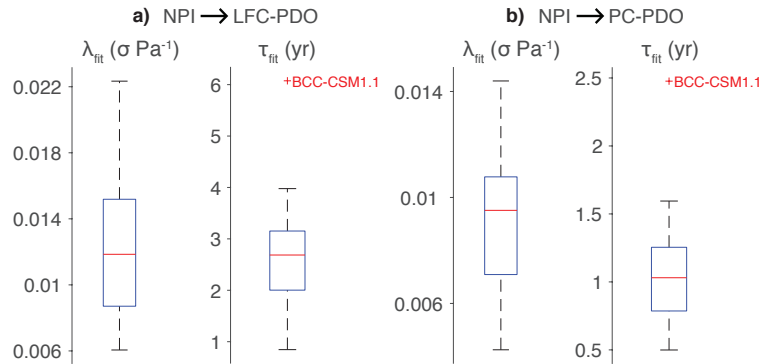

Figure S8. Distribution of best fit AR(1) parameters across CMIP5 models. (a) AR(1) fit to Aleutian Low forcing of LFC-PDO. (b) AR(1) fit to Aleutian Low forcing of PC-PDO. In each panel, the median is denoted with a red line, the box denotes the interquartile range, and the whiskers denote the full model range excluding outliers (outliers are fit parameters more than 1.5 times the interquartile range away from the box edges, shown in red).
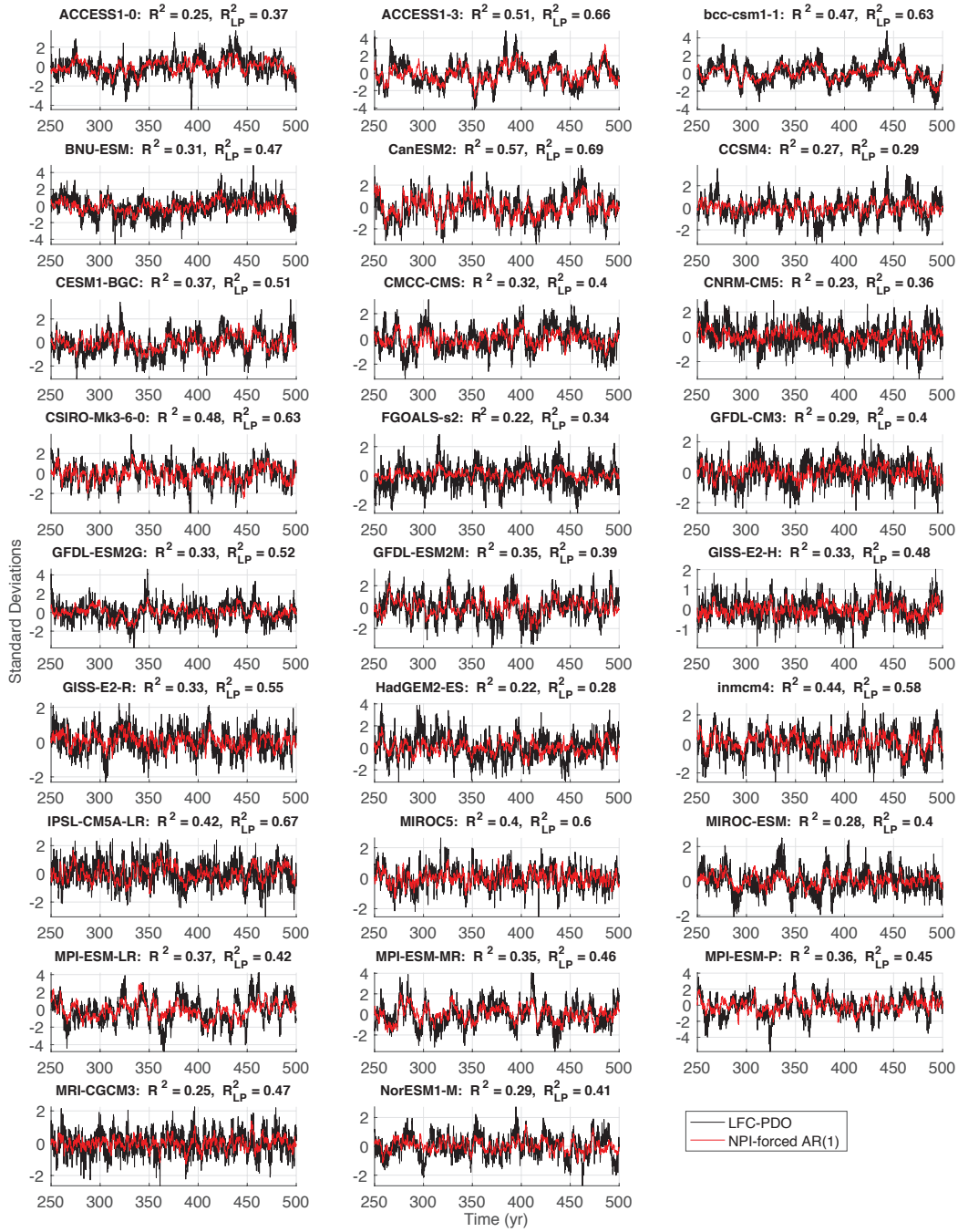
Figure S9. LFC-PDO time series for each model (black lines) and the best fit NPI forced AR(1) model [red lines, Eq. (1)], where the x-axes show time in years and the y-axes show anomalies in standard deviations. Fit parameters λ and τ are chosen to maximize the squared correlation (R^2) between the AR(1) model and the LFC-PDO. Fitting is done separately for each model. The R^2 and the squared correlation after 10-year lowpass filtering (R^2_{LP}) give measures of the goodness of fit.
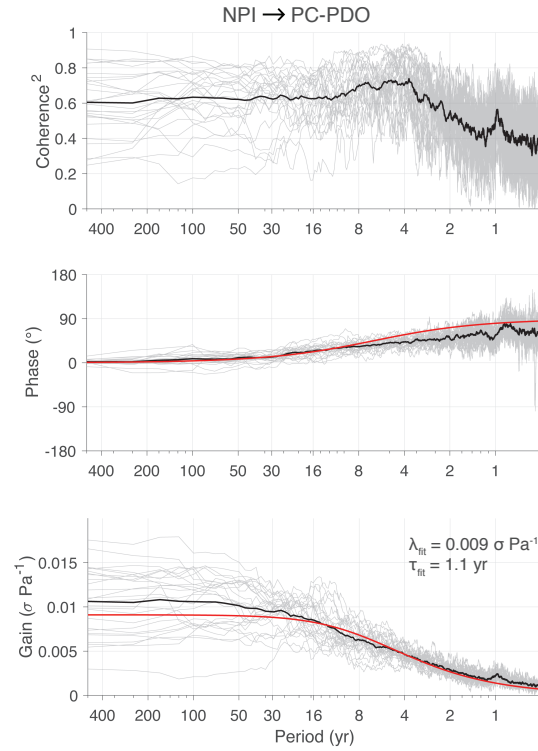
Figure S10. Spectral relationships between the Aleutian Low and PC-PDO and AR(1) model fit. Here the Aleutian Low is characterized by the North Pacific Index (NPI) (Trenberth & Hurrell, 1994). The top panel shows squared coherence. The middle panel shows phase (positive where PC-PDO lags NPI). The bottom panel shows the frequency response function or gain (i.e., the PC-PDO response per standard deviation NPI anomaly). Black lines show the multi-model mean; grey lines show individual models. Red lines show the AR(1) model fit.
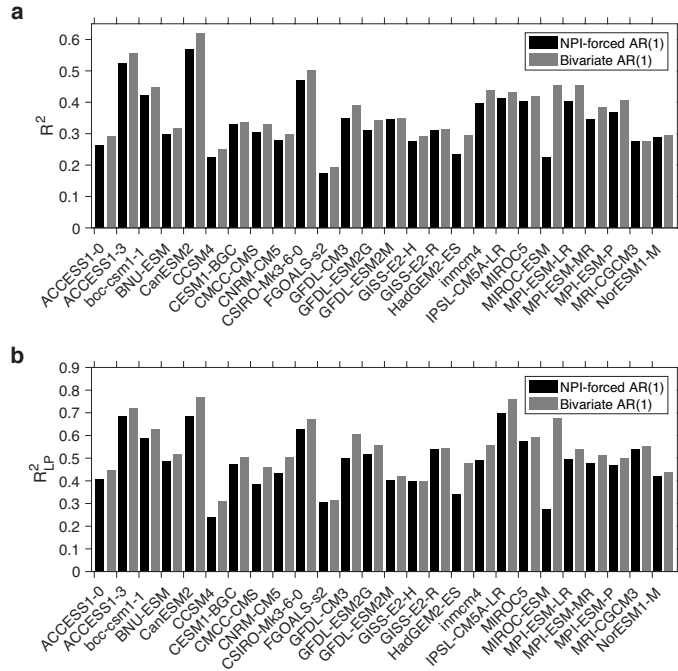
Figure S11. (a) R^2, the variance explained by the AR(1) model, computed separately for each CMIP5 model. (b) R^2_{LP}, the variance explained by the AR(1) model after applying a 10-year lowpass filter to the LFC-PDO and the AR(1) fits, computed separately for each CMIP5 model. The bivariate AR(1) model (dependent on NPI and ENSO) only slightly increases the variance explained compared to the univariate (NPI-forced) AR(1) model.

Table S1. CMIP5 pre-industrial control simulations used in this study and the 500 model years used from each. Models with dynamic sea-surface height data are denoted with an asterisk. Models with barotropic streamfunction data are denoted with a dagger.

Model	Model Years	Model	Model Years
ACCESS1.0*	300-799	GFDL-ESM2M*†	1-500
ACCESS1.3*	250-749	GISS-E2-H	2450-2949
BCC-CSM1.1	1-500	GISS-E2-R*†	4031-4530
BNU-ESM	1509-2008	HadGEM2-ES*	1935-2434
CanESM2*	2511-3010	INMCM4.0*†	1850-2349
CCSM4*†	801-1300	IPSL-CM5A*	2300-2799
CESM1-BGC	101-600	MIROC5*	2370-2869
CMCC-CMS*	3684-4183	MIROC-ESM*	1930-2429
CNRM-CM5*†	2200-2699	MPI-ESM-LR*†	2350-2849
CSIRO-Mk3.6.0*†	1-500	MPI-ESM-MR*†	2350-2849
FGOALS-s2	1851-2350	MPI-ESM-P*†	2506-3005
GFDL-CM3*†	1-500	MRI-CGCM3*†	1851-2350
GFDL-ESM2G*†	1-500	NorESM1-M*†	701-1200

References

Ebisuzaki, W. (1997). A method to estimate the statistical significance of a correlation when the data are serially correlated. *J. Climate*, *10*(9), 2147–2153.

Trenberth, K. E., & Hurrell, J. W. (1994). Decadal atmosphere-ocean variations in the Pacific. *Clim. Dyn.*, *9*(6), 303–319.